THE JOURNAL OF PHYSICAL CHEMISTRY C

Article

pubs.acs.org/JPCC

# Marangoni Flow Induced Collective Motion of Catalytic Micromotors

Manoj Manjare,*[,†] Fengchang Yang,[‡] Rui Qiao,[‡] and Yiping Zhao[†]

[†]Nanoscale Science and Engineering Center, Department of Physics and Astronomy, The University of Georgia, Athens, Georgia 30602, United States

[‡]Department of Mechanical Engineering, Virginia Polytechnic Institute and State University, Blacksburg, Virginia 24061, United States

Supporting Information

**ABSTRACT:** A new collective motion of non-bubble-propelled spherical Janus catalytic micromotors has been observed. When the local concentration of micromotors is high, bubbles start to form between the motors. As the bubble grows, micromotors move collectively toward the center of the bubble regardless of the orientations of their catalyst surface, eventually become aggregated, and captured around the perimeter of the bubble. It is suggested that this collective motion of the micromotors, too fast for the diffusiophoresis, can be caused by the entrainment of micromotors by the evaporation-induced Marangoni flow near the bubble. Numerical simulations confirmed that the direction and strength of such Marangoni flow are consistent with the fast, collective motion of micromotors observed experimentally.

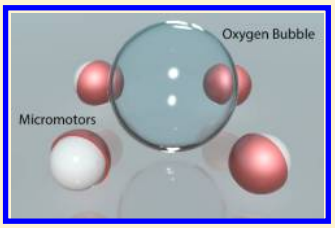


## 1. INTRODUCTION

In nature, one can observe two kinds of collective behaviors: swarming, in which individuals aggregate toward one common goal, and schooling, in which a group moves in unison in one direction at any point in time. Examples of swarming can be a group of predators hunting a prey or ants following other ants toward one food source. For schooling, a school of fish can move with incredible speed and agility in a group maintaining their grouping shape. They also change direction responding to environment instantaneously as a whole group. The collective behavior can happen only if there is a communication between the individuals of the group. It gives vast advantages to the members of the group to survive and prosper. These collective behaviors give rise to the so-called "emergent behavior", in which the communication within the group makes the movement appear to have an autonomy of its own. A key feature of this behavior is that there is no central command. No one individual is responsible for taking the decision for the whole group. Collective behaviors are also seen in the microscopic world. Bacteria move toward a food source or away from a harmful agent. Their preferential movement was first discovered and reported by Engelmann and Pfeffer in 1880.[1] This motion was termed as chemotaxis. The bacteria can sense the gradient in the concentration of chemicals and move toward the higher or lower concentration, depending on the nature of the chemicals. Gradually, an emergent behavior occurs as colonies of bacteria develop around a food source. The motion of bacteria could be considered as semi-autonomous since they are acting under an external chemical field but not totally controlled by the field. In nature, collective behavior is often driven by the nearest-neighbor interactions of independent mobile organisms.[2]

The collective motion behavior in artificial system is observed when artificial objects moving in response to external stimuli such as chemical gradients, electric fields, or magnetic fields. One particular system is catalytic micro/nanomotors. The catalytic micromotors, which use their catalytically functionalized surface to break down the fuel present in the surroundings for their motion, have come a long way since they were conceptualized and demonstrated by several groups.[3−7] These artificial motors that mimic the motion of their natural counterparts have surpassed the speed initially expected.[8,9] The catalytic micro/nanomotors in recent years showed many promising applications, such as delivering cargo, selectively detecting and targeting nucleic acids, etc.[10−15] In dilute suspensions, nanomotors move independently; however, when the concentration of motors becomes high, individual motors start to interact ("communicate") with each other and collective behaviors emerge.[2] Given that most of the emergent and collective behavior in nature is primarily driven by chemotaxis, the first account of nonbiological chemotaxis was reported by Hong et al. in 2007.[1] They used a hydrogel soaked with $H_2O_2$ and placed it in at the center of an enclosed chamber filled with Au−Pt nanorod motors. The gel slowly creates a concentration gradient in the chamber, with the highest concentration of $H_2O_2$ at the center and the lowest concentration at the edges of the chamber. They observed that the nanorods demonstrated autonomous motion but with temporal sensing. Over time, the nanorods accumulated toward the hydrogel due to "active diffusion". For bubble-propelled motors, especially microtube motors, collective behavior has been observed when motor concentration is increased substantially so that the motors are forced to operate with other motors in a very small space.[16] In the microtubes' case, the nearest-neighbor interactions arise due to proximity of other motors which leads to preferable surface attraction to

Received: May 11, 2015
Revised: November 23, 2015
Published: November 25, 2015





DOI: 10.1021/acs.jpcc.5b07251
J. Phys. Chem. C 2015, 119, 28361−28367

reduce surface tension. This emergent behavior of motors is complex and difficult to predict. However, it is clear that this collective motion of bubble propelled motors is not a direct result of the bubble growth and collapse dynamics.

Here, we report a new collective phenomenon of 5 $\mu$m diameter Janus catalytic motors (JCMs) induced by bubble nucleation, growth, and collapse among a group of motors wherein ringlike assemblies are spontaneously formed in an $H_2O_2$ environment. Specifically, when the JCMs are introduced in a reservoir containing $H_2O_2$, they initially perform autonomous diffusiophoretic motion. However, when multiple JCMs are randomly crowded into a small region, bubbles start to nucleate. When a single bubble is nucleated, it starts the process of collective motion. During its growth, the bubble forces the participating JCMs to arrange around its base in a ringlike structure and draws them toward the center of the ring in a coordinated fashion, until the bubble collapses. This process repeats until the fuel is exhausted. The dynamics of the process are much different from the previously reported collective/schooling behaviors and bubble propulsion among micromotors. This process is not activated by any external chemical or light trigger, and it occurs spontaneously. It is a result of bubble nucleation, growth, and collapse. This motion has been observed to occur more readily if the noncatalyst surface of the motors is made hydrophobic. Such multifaceted motion—trigger-free schooling, transition between diffusiophoresis and bubble propulsion, periodic motion, collective bubbling among micromotors—has not been previously reported to the best of our knowledge.

## 2. RESULTS AND DISCUSSION

A droplet of suspension loaded with JCMs was first deposited on clean Si and observed under the microscope. Another droplet of 10−20% $H_2O_2$ solution was then added to the first droplet. For the high concentration ($3 \times 10^5$ motors/mL) 5 $\mu$m JCM suspended in the $H_2O_2$ solution, no bubbles are observed initially, and the JCMs exhibit autonomous diffusiophoretic motion.[17,18] However, after a short period of time (~30−60 s), when motors drift randomly in the droplet, sometimes more than 2 or 3 JCMs come very close to each other. This type of "aggregation" is assumed to be random since it is observed to occur repeatedly at different locations in the liquid film. Once the JCMs come close to each other, a visible bubble starts to form in between JCMs. The bubble forces the adjacent JCMs to arrange at its base in a circle. As the bubble grows, it draws the JCMs in its vicinity toward the center of the circle. Once the bubble grows to a critical $R_{max}$ (typically between 50 and 75 $\mu$m), it collapses. However, the circular ring of JCMs is maintained, and a new bubble starts to nucleate at the center of the ring and the above process repeats until the fuel is exhausted. The number of JCMs that can induce such a phenomenon is arbitrary, as shown in the movies in the Supporting Information (Movies 1−6). Figure 1 is a series of snapshots of a video taken during this process. It shows the process of initial swarming of JCMs, the bubble growth, and then the new bubble nucleation after previous one has collapsed. The new bubble also reaches approximately the same radius, $R_{max}$, before it collapses, and the cycle continues. It is important to note that the bubble is not attached to the surface of any JCMs, and all the JCMs seem to collectively feed the bubble with $O_2$ from their catalytic conversion of $H_2O_2$. As the time stamps indicate, the bubble growth−collapse cycles can be very fast. In 1 s, as many as 20−30 cycles of bubble growth and collapse can be observed, and the JCM's speed during those cycles can reach a few hundred $\mu$m/s. However, we note that slower cycles which take up to 1 s are also observed. The expected motion of JCMs due to diffusiophoresis, which is to travel in the opposite direction of the catalyst surface, is ceased, and the micromotors are locked in these ring structures. Figure 2a shows the snapshot of a video sequence at a moment when the initial bubble of the cycle has just collapsed. Superimposed are the trajectories that each JCM motor follows after this image was taken. The red arrows denote the directions of the JCM motions. The JCMs all travel approximately toward a common point, which is the center of the bubble. This can be seen more clearly by examining the histograms of the displacement of each JCM. Specifically, for each JCM, we defined the line pointing from the center of bubble to the center of the JCM as the radial direction. We then decomposed the JCM's displacement during one bubble growth−burst cycle into a radial and a tangential component. As shown in Figure 2b, the histogram of these two displacement components demonstrates that the net displacement of JCMs is toward the bubble center. The bubble itself is not necessarily fixed to a location on Si substrate and is sometimes observed to move in the horizontal plane, with the ring moving with it. For example, in Movie 3, the bubbles move laterally with a translation speed varying from 20 to 60 $\mu$m/s depending on the ring size. The figure shows a few interesting features: (1) All the motors are arranged and locked in a virtual circle. (2) None of the motors are physically attached to the bubble, which suggests that all or most of the JCMs are feeding $O_2$ to the bubble remotely. The bubble seems to feed from the surrounding supersaturated $O_2$. (3) Regardless of orientation of JCMs, their motions are mostly radial, which suggests that the diffusiophoresis is unimportant, as demonstrated in the movies (see Supporting Information). The average number of JCMs required to instigate the above collective motion is investigated as a function of JCM density $\rho$ in the suspension (from $7 \times 10^4$ to $3 \times 10^5$ motors/mL) of two different JCMs, hydrophilic JCMs, and hydrophobic JCMs.[19] For hydrophilic JCMs, the collective behavior only occurred at the highest motor density $\rho = 3 \times 10^5$ motors/mL. For hydrophobic JCMs, all the densities produced swarming and collective bubbling. The average number of motors taking part in the collective bubbling differs significantly for hydrophobic and hydrophilic JCMs. Figure 3 shows a plot of the average number of JCMs in a ring as a function of JCM density $\rho$. For hydrophobic JCMs, the average number of beads in the ring decreases monotonically with $\rho$. However, for hydrophilic JCMs, the number of beads in the ring is significantly more than the highest bead average for hydrophobic JCMs. This indicates that the number of beads required for collective bubbling is less for hydrophobic JCMs than for hydrophilic ones. This difference in the behavior of hydrophilic and hydrophobic motors is caused by difference in reaction dynamics at the Pt boundaries of both types of motors

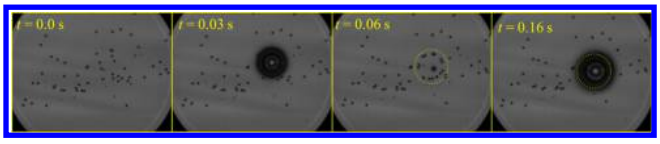


**Figure 1.** Snapshots of JCMs as they get densely populated in a small region and the subsequent bubble and ring formations. The small black dots are the 5 $\mu$m diameter JCMs.


DOI: 10.1021/acs.jpcc.5b07251
J. Phys. Chem. C 2015, 119, 28361−28367

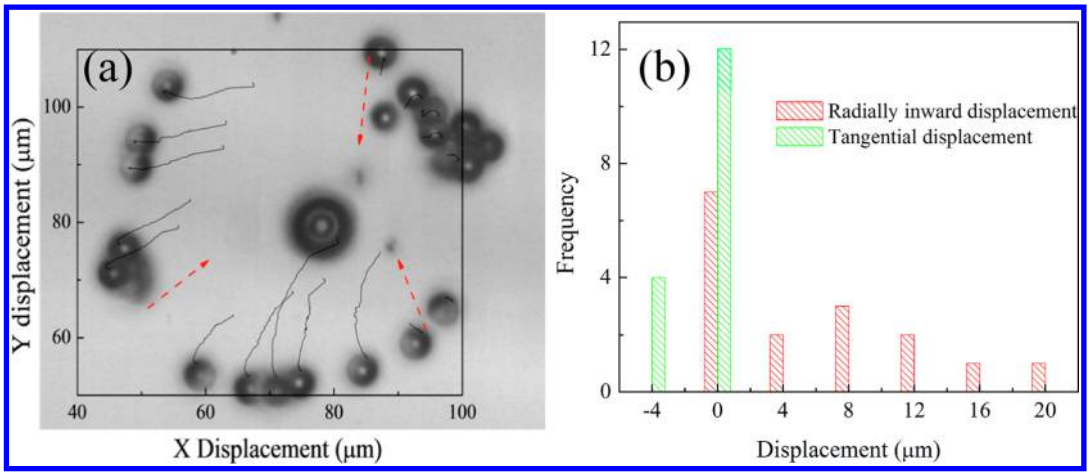


**Figure 2.** After the initial bubble collapse, the JCMs are locked in a ring. They all travel toward the center of the bubble as it grows. (a) Screenshot of an instant when new bubble starts to grow. The black lines highlight the trajectory of each motor. (b) Histogram of the decomposed displacements of JCMs in the radial and the tangential directions (for each JCM, the line pointing from the center of bubble to the center of the JCM is defined as the radial direction).

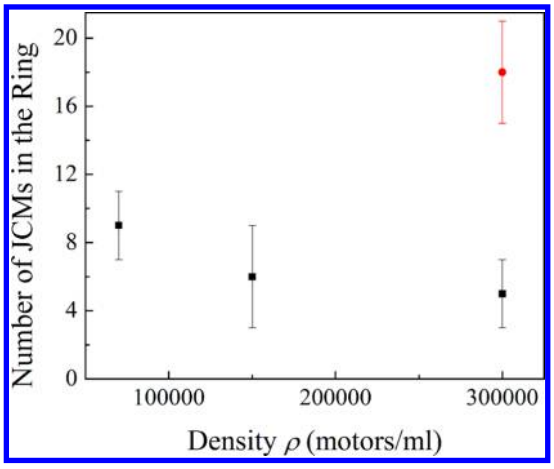


**Figure 3.** Number of JCMs in the ring for different densities of motors/mL. Square symbols represent the hydrophobic JCMs, and the round symbols represent hydrophilic JCMs.

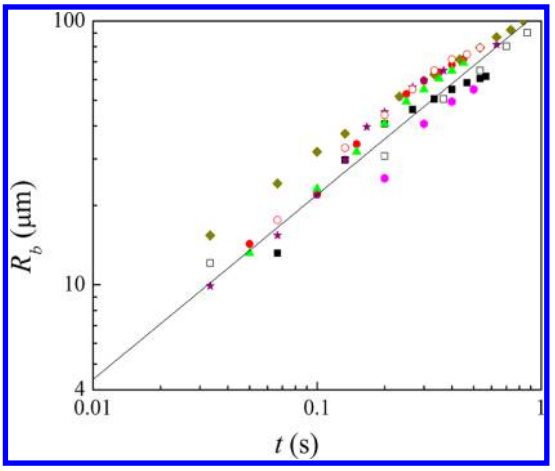


**Figure 4.** A log−log plot of the bubble growth radius $R_b$ as a function of time $t$ for different groups (hydrophobic and hydrophilic) of motors. Each different symbol represents a new bubble cycle. The red dotted line represents the power law fitting $R_b \sim t^n$ with $n = 0.7$.

and is discussed later. Once a bubble forms between several JCMs, its growth is fed by the diffusion of oxygen generated on the surfaces of these JCMs. Figure 4 shows that the growth of bubble follows a power law,[20] i.e., $R_b \sim t^n$, with $n = 0.7 \pm 0.2$, for all cases we observed. Such a growth law differs significantly from that for bubbles attached to single JCMs, where $n$ is typically ~0.33 due to the nearly constant feed of oxygen into bubble.[17,18] The growth law observed here also differs from the growth of bubbles in homogeneous fluids supersaturated with oxygen, where $R_b \sim t^{0.5}$. The more linear growth of the bubbles observed here is likely due to the fact that during the growth of the bubble, JCMs (i.e., the source of oxygen for bubble growth) moves toward its base, thereby making the transport of oxygen into bubble easier.

As established in previous reports,[17,18] no bubbles can be observed on individual 5 $\mu$m JCM beads. The critical nucleation energy cannot be reached on the surface of these motors for several reasons. One of the most important reasons is the concentration of $O_2$ in locations between the JCMs. For a single 5 $\mu$m JCM, the $O_2$ concentration near the surface of JCM could not easily reach the critical value for bubble nucleation, nor does the $O_2$ concentration away from the surface due to the limited amount of $O_2$ produced by the available catalyst surface area. The diffusiophoretic motion of the JCM also prevents the $O_2$ from accumulating and reaching the critical value. However, the limitation can be overcome if a group of JCMs are placed in a favorable environment. When more than two JCMs are arranged in a ring with small diameter, it is expected that the $O_2$ production will naturally go up due to the number of the JCMs. Additionally, it also becomes harder for $O_2$ molecules inside the ring area to escape, since the concentration of $O_2$ is highest at the circumference of the ring and lowest at the center, effectively restricting the diffusion of $O_2$ away. This helps the concentration of $O_2$ between the JCMs reaching the saturation concentration faster. In fact, a higher $O_2$ flux is evident when the bubble growth dynamics is examined.

Although the collective motion has been studied in detail in biological systems and many theoretical models have been proposed to explain such motion,[21] the same approach could not be used for the phenomenon we observed. The collective motion of the JCMs is synchronized with the bubble growth and collapse cycles. As noted before, the orientation of motors does not influence the motion. This implies that diffusiopho-


DOI: 10.1021/acs.jpcc.5b07251
J. Phys. Chem. C 2015, 119, 28361−28367

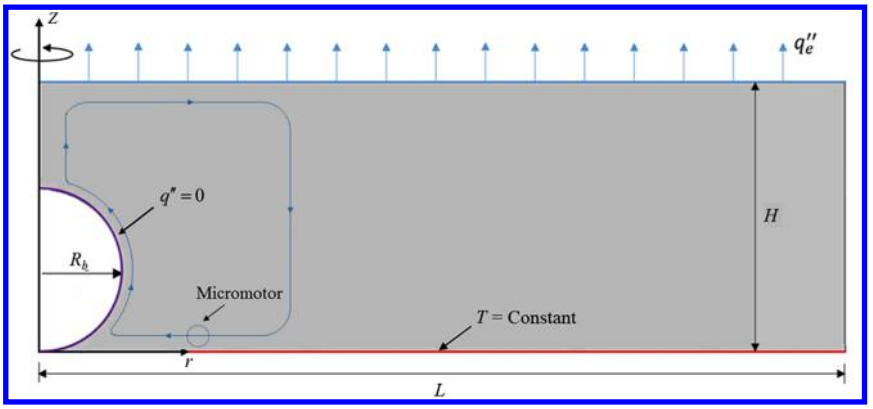


**Figure 5.** Schematic of the evaporation-induced Marangoni flow. Cooling via evaporation at top surface of the liquid film creates a temperature gradient along bubble surface. Such a temperature gradient generates a Marangoni stress on bubble surface, which in turn induces a Marangoni flow in the vicinity of bubble.

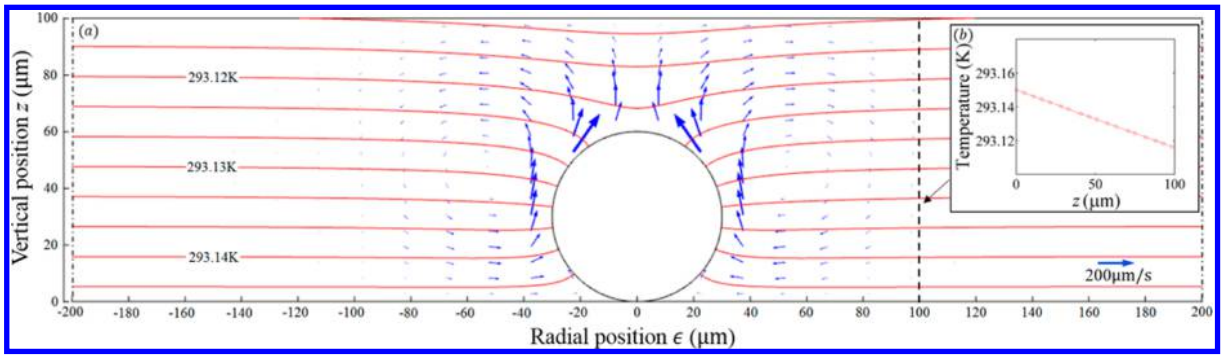


**Figure 6.** Marangoni flow in the vicinity of the bubble within a cooling liquid film. (a) Velocity field (blue vectors) and temperature contours (red lines) are calculated for a bubble radius of 30 $\mu$m. The thickness of the liquid film is 100 $\mu$m, and a uniform cooling flux of 200 W/m$^2$ is applied on liquid film surface. (b) Temperature profile across the liquid film at a radial position of 100 $\mu$m.

resis is not the dominant driving mechanism. The motion analysis of JCMs observed during bubble growth indicates that JCMs move toward the bubble's base with a speed up to a few hundred of $\mu$m/s. Such a collective movement of the JCMs is too fast to be caused by the diffusiophoresis mechanism.[22,23] The collective movement of JCM can also be due to the entrainment by bubble growth-induced flows, but calculations (see Figure S3 in the Supporting Information) indicated that entrainment due to such flow ($\sim O(1\ \mu$m/s)) is too weak to explain the fast movement of JCMs observed experimentally. We hypothesize that the fast movement of JCMs toward bubble's base is caused by evaporation induced Marangoni flow near the bubble since the observing liquid drop is thin ($\sim$100 $\mu$m) on Si substrates. As shown in Figure 5, the evaporation of water on the top surface of the liquid film induces a heat flux, $q_e''$, which causes the liquid at the bottom of bubble to be warmer than that at the top of the bubble. Since the surface tension of water decreases as temperature increases, the surface tension of water is higher at top of the bubble than at the bottom of the bubble. This variation of the surface tension along the bubble surface drives a Marangoni flow,[24] which can entrain JCMs near the substrate toward the bubble's base. Previous studies indicate that the evaporation rate at the surface of droplet and thin liquid films is governed by the diffusion of water vapor from the liquid−air interface toward the surrounding atmosphere, and the air at liquid film surface is saturated by water.[25] Therefore, for the thin liquid film containing the JCMs, the average cooling rate $q_e''$ on its top surface due to evaporation is given by

$$q_e'' = h_w \dot{m}_{eva} \quad \text{and} \quad \dot{m}_{eva} = D\frac{S}{\pi {R_f}^2} {C_w}^*(1-\varphi) \tag{1}$$

where $R_f$ is the radius of thin liquid film, $h_w$ is the latent heat of water, $S = 4R_f$ is the shape factor for mass diffusion from a thin film of radius $R_f$ toward a semi-infinite domain,[26] $D$ is the diffusion coefficient of water vapor in air, $C_w^*$ is the saturation concentration of water in air, and $\varphi$ is the relative humidity of surrounding atmosphere. In the present experiments, the water film on the substrate has a radius of $\sim$5 mm. Hence, the cooling flux is $q_e''$ = 200 W/m$^2$ if the relative humidity of the surrounding environment is 50% and the thermophysical properties of water at room temperature are used ($k$ = 0.563 W/(m.K), $D = 2.82 \times 10^{-5}$ m$^2$/s, and $h_w$ = 2260 kJ/kg). This cooling heat flux generates a temperature gradient along bubble surface, which in turn leads to a surface tension gradient (i.e., Marangoni stress) and flow along the bubble surface.

To quantify the strength of the evaporation-induced Marangoni flow, we simulate such flow near a single bubble under the axisymmetric condition as sketched in Figure 5. The bubble is treated as spherical, attached to the substrate with an approximately zero contact angle. Since the Marangoni flow mainly exists in the vicinity of bubble, we set the length of the simulation domain, $L$, to be 300 $\mu$m (using a larger length only changes the result slightly). The thickness of liquid film, $H$, is set as 100 $\mu$m, similar to that in our experiments. Since the dimension of simulation domain is much smaller than the liquid film, the top surface of the simulation domain can be treated as flat.[27] On the basis of this setup, we solve the thermal and fluid


DOI: 10.1021/acs.jpcc.5b07251
J. Phys. Chem. C 2015, 119, 28361−28367

transport inside water (i.e., outside of the bubble; see the shaded region in Figure 5) (see Methods section) and obtained the velocity and temperature fields near a bubble attached to the substrate during bubble growth. Figure 6 shows the velocity and temperature fields at the moment when bubble radius $R_b$ is 30 $\mu$m. We observed that the cooling at the top surface of the liquid film induces a temperature gradient along bubble surface. This temperature gradient generates a strong Marangoni flow in the vicinity of the bubble. The magnitude of the Marangoni flow is on the order of $O(100\ \mu m/s)$, which is consistent with our observations above. Figure 6 shows that the Marangoni flow at positions near the substrate is directed toward the bubble base, which can potentially entrain JCMs toward the bubble. To more quantitatively examine the entrainment of JCMs by the Marangoni flow, we plot the radial velocity of the Marangoni flow at a distance of 5 $\mu$m above the substrate (see Figure 7), where the JCMs are observed in our experiments. A

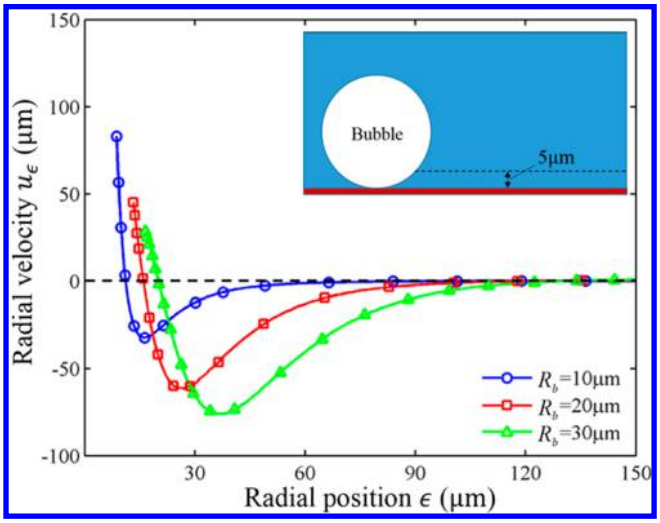


**Figure 7.** Radial velocity of the Marangoni flow in the vicinity of a bubble. Flow velocities are evaluated at a position of 5 $\mu$m above the substrate (dashed line in the inset). The thickness of the liquid film is 100 $\mu$m, and a uniform cooling flux of 200 W/m$^2$ is applied on the film surface. The negative velocity corresponds to the flow toward the bubble base.

positive/negative velocity means the flow is directed outward/toward bubble base. Figure 7 shows that except in the immediate vicinity of bubble surface, the fluid moves toward bubble base. For example, for a bubble with a radius of 10 $\mu$m, fluids movement toward bubble base with a speed $\sim O(10\ \mu m/s)$ exists in the region $\sim 2R_b$ from the bubble surface. As the bubble grows larger, the flow that can entrain JCMs enhances, but its speed remains $\sim O(10-100\ \mu m/s)$; the region within which JCMs are strongly entrained remains $\sim 2R_b$. We note that there exists a region in the immediate vicinity of bubble surface, where the radial velocity is positive. This positive velocity corresponds to the deflection of the fluid flow by the bubble surface (Figure 5). From Figures 6 and 7, we find that the direction and speed $\sim O(10-100\ \mu m/s)$ of the evaporation-induced Marangoni flow predicted in our simulation help explain the fast, collective movement of JCMs toward the bubble base.

Even though the Marangoni flow mechanism is similar for both hydrophobic and hydrophilic JCMs, the large differences between the collective behavior in hydrophobic and hydrophilic JCMs as highlighted in Figure 3 could be explained by the difference in $O_2$ supersaturation in the two cases. The catalytic conversion rate of Pt on the hydrophobic JCM is effectively larger than that for the hydrophilic JCM. This is because of the depletion later formed around the Pt surface that allows quick removal of $O_2$ from Pt surface and dispersion into the liquid.[19] This causes the catalytic reaction rate on Pt surface surrounded by a hydrophobic surface to be greater than that of the Pt surface surrounded by a hydrophilic surface. Thus, the speed of 5 $\mu$m hydrophobic JCM is about 1.8 times that of the hydrophilic JCMs.[19] For the collective behavior observed in our experiments, this results in a quick buildup of overall $O_2$ concentration inside the ring for the hydrophilic JCMs, which can raise the $O_2$ concentration to near its saturation concentration for bubble nucleation with fewer number of JCMs, as seen in Figure 3.

As the Marangoni effects are induced by the evaporation of water at the top surface of the liquid film, whose intensity is controlled by the relative humidity of the surround air (see eq 1), we expect that the collective motion of JCMs to be suppressed if the relative humidity of the air is increased. Preliminary experiments were performed to confirm this claim by placing the entire liquid film loaded with micromotors inside a glass enclosure sealed by a glass slide. The bottom portion of the glass enclosure was filled with warm water to increase the humidity and prevent liquid evaporation. We did observe that the collective bubbling effect disappeared, which supports our hypothesis that the Marangoni effects are responsible for the collective motion of JCMs observed in Figures 1 and 2. We note that if the motors were located at the air−liquid interface, the collective motion could have been explained by capillary forces.[16,28] To confirm that capillary forces are not involved in the behavior of motors, we ensure that the motors are fully immersed in our experiments. As also seen in Movie 2, we made scratches on the Si substrate and made sure that they and the motors are in focus at the 50× objective.

## 3. CONCLUSION

In conclusion, we have observed a new collective motion behavior of JCMs accompanied by periodic bubbling. The individual 5 $\mu$m JCM is not driven by bubble-propelled mechanism. However, at high JCM density, JCMs aggregate locally and collectively enable the nucleation and growth of bubbles. As bubble grows, the JCMs exhibit a collective, synchronized motion. This motion is fast, and its direction is toward the center of the bubble, regardless of the orientation of catalytic surface on the JCMs. It is proposed that the motion of motors toward the bubble center is caused by the Marangoni flow effects. Our numerical simulations show that the Marangoni effect can produce similar speeds observed in the experiments. The collective motion should also be observed for other catalytic particles. This is because the formation of bubble and consequently the Marangoni flow near the bubble should exist as long as gas molecules are released from the surface of catalytic particles, regardless whether the particle is half-coated or fully coated with catalysts. The higher effective conversion rate of $H_2O_2$ at the catalytic surface of hydrophobic JCM results in easier $O_2$ saturation and bubble formation than in the hydrophilic JCMs. This result could be expected to garner interest for collective task management with fewer size restrictions as far as bubble nucleation is concerned.


DOI: 10.1021/acs.jpcc.5b07251
J. Phys. Chem. C 2015, 119, 28361−28367

## 4. EXPERIMENTAL AND SIMULATION METHODS

**Experiments.** For this study we use JCM motors with a 5.2 $\mu$m diameter. The JCM motors are divided into two groups: hydrophobic motors and hydrophilic motors (note: only the non-Pt side is functionalized). The fabrication process is the same as described in previous reports.[19] We start with commercially available silica microspheres (Catalog No. SS06N, Bangs Laboratories). The hydrophobic motors are achieved by using heptadecafluoro-1,1,2,2-tetrahydrodecyl-trichlorosilane (HFTS) (catalog no. SIH5841, Gelest, Inc.) to coat the entire surface of silica microspheres and then using electron beam deposition to coat 10 nm Ti adhesion layer and 30 nm Pt on one-half surfaces of the microspheres. The hydrophilic motors are achieved by using pristine silica microspheres and coating Ti and Pt on one-half surface (skipping the HFTS coating). After the motors are fabricated, they are suspended in 18 MΩ·cm deionized water by ultrasonication. For the experiments, a droplet (5 $\mu$L) containing a few beads is cast on a clean Si surface and observed under the microscope. 10−20% peroxide (5 $\mu$L) is then added to the droplet. The spread of the reservoir is about 10 mm in diameter. This makes the ceiling of the reservoir approximately 100 $\mu$m tall. The volume of the droplet selected is such that the resulting reservoir does not evaporate quickly and can be changed without affecting the quality of observations. The observation and recording protocols mentioned in previous reports are followed.[17,19] The motion of the JCMs is recorded at different speeds depending on the detail required (for trajectories, 25 frames/s and bubble growth collapse cycles, 1000−10 000 frames/s recording speeds were used), with a CCD camera (Phantom v9.1) using 10× and 50× magnification objective lens of a Mitituya FS110 microscope.

**Simulations.** Figure 5 shows a schematic of the simulation setup for studying the evaporation-induced Marangoni flows. The simulation system features a single bubble attached to a substrate covered by a thin liquid film. To simulate the fluid flow and heat transfer near the bubble, the temperature and flow fields are assumed to be at quasi-steady state during the growth of bubble. This is a good approximation because both the Peclet and Reynolds numbers are small.[29] Specifically, in our case, using the bubble radius as the characteristic length scale ($R_b \sim O(10\ \mu m)$) and the JCM velocity as the characteristic velocity scale ($U \sim O(100\ \mu m/s)$), we have the Peclet number $Pe \sim O(10^{-2})$ and the Reynolds number $Re \sim O(10^{-3})$. Under the quasi-steady-state conditions, the temperature field observes the Laplace equation, and the flow field observes the Stokes equations. In the heat transfer model, zero heat flux is applied on the bubble surface. The temperature on the substrate is set to $T_s$ = 293.15 K. Generally, the cooling flux on the surface of a finite-sized liquid film/droplet is nonuniform, which plays a key role in generating the Marangoni flow that spans the entire liquid film/droplet.[30−32] However, in this study, we neglect this nonuniformity and implement the uniform cooling flux of $q''_e$ = 200 W/m$^2$ computed in the main text. Such a treatment is reasonable here for two reasons. First, because the water film has a much larger radius compared to the bubble and most bubbles are positioned away from the edge of the film, the cooling flux on surface of the water film near these bubbles is rather uniform. Second, the nonuniformness of the cooling on the surface of liquid film only weakly affects the Marangoni flow *near the bubble*, the focus of the present study. To capture the flow induced by the Marangoni stress and growth of bubble, the bubble surface moves with a speed measured from experiments, and an extra Marangoni stress due to the temperature gradient is added to both bubble surface and the liquid film surface. The substrate is set as a no-slip and impermeable wall. The mathematical models for the fluid and thermal transport problem described above were solved using a finite element package COMSOL.[33] Equations for these mathematical models and their implementation in COMSOL are summarized in the Supporting Information.

## ■ ASSOCIATED CONTENT

### Supporting Information

The Supporting Information is available free of charge on the ACS Publications website at DOI: 10.1021/acs.jpcc.5b07251.

Bubble behavior by JCMs (AVI)
Bubble behavior by JCMs (AVI)
Bubble behavior by JCMs (AVI)
Bubble behavior by JCMs (AVI)
Bubble behavior by JCMs (AVI)
Bubble behavior by JCMs (AVI)
Details of the mathematical models and their numerical implementation and results on fluid flow induced by the growth of bubbles (PDF)

## ■ AUTHOR INFORMATION


### Corresponding Author

*E-mail manojative@physast.uga.edu (M.M.).


### Notes

The authors declare no competing financial interest.

## ■ ACKNOWLEDGMENTS

The authors gratefully acknowledge support by the National Science Foundation (ECCS-1303134 and ECCS-1464146).

## ■ REFERENCES


(1) Hong, Y.; Blackman, N.; Kopp, N.; Sen, A.; Velegol, D. Chemotaxis of Nonbiological Colloidal Rods. *Phys. Rev. Lett.* **2007**, *99*, 178103.

(2) Wang, W.; Duan, W.; Ahmed, S.; Mallouk, T. E.; Sen, A. Small Power: Autonomous Nano- and Micromotors Propelled by Self-Generated Gradients. *Nano Today* **2013**, *8*, 531−554.

(3) Ismagilov, R. F.; Schwartz, A.; Bowden, N.; Whitesides, G. M. Autonomous Movement and Self-Assembly. *Angew. Chem., Int. Ed.* **2002**, *41*, 652−676.

(4) Paxton, W. F.; Kistler, K. C.; Olmeda, C. C.; Sen, A.; St. Angelo, S. K.; Cao, Y. Y.; Mallouk, T. E.; Lammert, P. E.; Crespi, V. H. Catalytic Nanomotors: Autonomous Movement of Striped Nanorods. *J. Am. Chem. Soc.* **2004**, *126*, 13424−13431.

(5) Wang, J.; Manesh, K. M. Motion Control at the Nanoscale. *Small* **2010**, *6*, 338−345.

(6) Mei, Y.; Huang, G.; Solovev, A. A.; Ureña, E. B.; Mönch, I.; Ding, F.; Reindl, T.; Fu, R. K. Y.; Chu, P. K.; Schmidt, O. G. Versatile Approach for Integrative and Functionalized Tubes by Strain Engineering of Nanomembranes on Polymers. *Adv. Mater.* **2008**, *20*, 4085−4090.

(7) Mei, Y. F.; Solovev, A. A.; Sanchez, S.; Schmidt, O. G. Rolled-Up Nanotech On Polymers: From Basic Perception To Self-Propelled Catalytic Microengines. *Chem. Soc. Rev.* **2011**, *40*, 2109−2119.

(8) Sanchez, S.; Ananth, A. N.; Fomin, V. M.; Viehrig, M.; Schmidt, O. G. Superfast Motion of Catalytic Microjet Engines at Physiological Temperature. *J. Am. Chem. Soc.* **2011**, *133*, 14860−14863.




DOI: 10.1021/acs.jpcc.5b07251
J. Phys. Chem. C 2015, 119, 28361−28367

(9) Gao, W.; Sattayasamitsathit, S.; Wang, J. Catalytically Propelled Micro-/Nanomotors: How Fast Can They Move? *Chem. Rec* **2012**, *12*, 224−231.
(10) Kagan, D.; Laocharoensuk, R.; Zimmerman, M.; Clawson, C.; Balasubramanian, S.; Kang, D.; Bishop, D.; Sattayasamitsathit, S.; Zhang, L.; Wang, J. Rapid Delivery Of Drug Carriers Propelled and Navigated By Catalytic Nanoshuttles. *Small* **2010**, *6*, 2741−2747.
(11) Orozco, J.; Cortes, A.; Cheng, G. Z.; Sattayasamitsathit, S.; Gao, W.; Feng, X. M.; Shen, Y. F.; Wang, J. Molecularly Imprinted Polymer-Based Catalytic Micromotors for Selective Protein Transport. *J. Am. Chem. Soc.* **2013**, *135*, 5336−5339.
(12) Sundararajan, S.; Sengupta, S.; Ibele, M. E.; Sen, A. Drop-Off Of Colloidal Cargo Transported by Catalytic Pt-Au Nanomotors Via Photochemical Stimuli. *Small* **2010**, *6*, 1479−1482.
(13) Wang, J.; Kagan, D.; Campuzano, S.; Balasubramanian, S.; Kuralay, F.; Flechsig, G. U. Functionalized Micromachines for Selective and Rapid Isolation of Nucleic Acid Targets from Complex Samples. *Nano Lett.* **2011**, *11*, 2083−2087.
(14) Yadav, V.; Freedman, J. D.; Grinstaff, M.; Sen, A. Bone-Crack Detection, Targeting, and Repair Using Ion Gradients. *Angew. Chem., Int. Ed.* **2013**, *52*, 10997−11001.
(15) Wu, J.; Balasubramanian, S.; Kagan, D.; Manesh, K. M.; Campuzano, S.; Wang, J. Motion-Based DNA Detection Using Catalytic Nanomotors. *Nat. Commun.* **2010**, *1*, 1.
(16) Solovev, A. A.; Sanchez, S.; Schmidt, O. G. Collective Behaviour of Self-Propelled Catalytic Micromotors. *Nanoscale* **2013**, *5*, 1284−1293.
(17) Manjare, M.; Yang, B.; Zhao, Y. P. Bubble Driven Quasioscillatory Translational Motion of Catalytic Micromotors. *Phys. Rev. Lett.* **2012**, *109*, 128305.
(18) Huang, W. J.; Manjare, M.; Zhao, Y. P. Catalytic Nanoshell Micromotors. *J. Phys. Chem. C* **2013**, *117*, 21590−21596.
(19) Manjare, M.; Wu, Y. T.; Yang, B.; Zhao, Y. P. Hydrophobic Catalytic Janus Motors: Slip Boundary Condition and Enhanced Catalytic Reaction Rate. *Appl. Phys. Lett.* **2014**, *104*, 054102.
(20) Thorncroft, G. E.; Klausner, J. F.; Mei, R. An Experimental Investigation of Bubble Growth and Detachment in Vertical Upflow and Downflow Boiling. *Int. J. Heat Mass Transfer* **1998**, *41*, 3857−3871.
(21) Mehes, E.; Vicsek, T. Collective Motion Of Cells: From Experiments To Models. *Integr Biol-Uk* **2014**, *6*, 831−854.
(22) Gibbs, J. G.; Zhao, Y. P. Autonomously Motile Catalytic Nanomotors by Bubble Propulsion. *Appl. Phys. Lett.* **2009**, *94*, 163104.
(23) Howse, J. R.; Jones, R. A. L.; Ryan, A. J.; Gough, T.; Vafabakhsh, R.; Golestanian, R. Self-Motile Colloidal Particles: From Directed Propulsion To Random Walk. *Phys. Rev. Lett.* **2007**, *99*, 048102.
(24) Young, N.; Goldstein, J.; Block, M. The Motion Of Bubbles an a Vertical Temperature Gradient. *J. Fluid Mech.* **1959**, *6*, 350−356.
(25) Hu, H.; Larson, R. G. Evaporation of a Sessile Droplet on a Substrate. *J. Phys. Chem. B* **2002**, *106*, 1334−1344.
(26) Incropera, F. P. *Fundamentals of Heat and Mass Transfer*; John Wiley & Sons: 2011.
(27) O'Shaughnessy, S. M.; Robinson, A. J. Numerical Investigation of Bubble Induced Marangoni Convection: Some Aspects of Bubble Geometry. *Microgravity Sci. Technol.* **2008**, *20*, 319−325.
(28) Velev, O. D.; Denkov, N. D.; Paunov, V. N.; Kralchevsky, P. A.; Nagayama, K. Direct Measurement of Lateral Capillary Forces. *Langmuir* **1993**, *9*, 3702−3709.
(29) Anderson, J. L. Droplet Interactions in Thermocapillary Motion. *Int. J. Multiphase Flow* **1985**, *11*, 813−824.
(30) Hu, H.; Larson, R. G. Analysis of the Effects of Marangoni Stresses on the Microflow in an Evaporating Sessile Droplet. *Langmuir* **2005**, *21*, 3972−3980.
(31) Bhardwaj, R.; Fang, X.; Attinger, D. Pattern Formation During the Evaporation of a Colloidal Nanoliter Drop: a Numerical and Experimental Study. *New J. Phys.* **2009**, *11*, 075020.
(32) Yunker, P. J.; Still, T.; Lohr, M. A.; Yodh, A. Suppression of the Coffee-Ring Effect by Shape-Dependent Capillary Interactions. *Nature* **2011**, *476*, 308−311.
(33) Comsol, A. COMSOL Multiphysics User's Guide. Version: September 2005.



DOI: 10.1021/acs.jpcc.5b07251
*J. Phys. Chem. C* 2015, 119, 28361−28367